Investigating renewable fuel combusion II: DNS of DME and n-heptane ignition in a turbulent non-homogeneous flow with high dissipation

Boulanger, J.; Liu, F.; Neill, W. S.; Smallwood, G. J.

Publisher's version / Version de l'éditeur:
https://doi.org/10.1080/00207230701382040
International Journal of Environmental Studies, 64, 4, pp. 419-432, 2007

Investigating Renewable Fuel Combustion. II: DNS of DME and n-Heptane Ignition in a Turbulent non-Homogeneous Flow with High Dissipation.

Joan Boulanger[+], Fengshan Liu, W. Stuart Neill and Gregory J. Smallwood

Institute for Chemical Process and Environmental Technology

and [+]Gas Turbine Laboratory, Institute for Aerospace Research

National Research Council Canada, 1200 Montréal Road, Ottawa, Ontario, Canada, K1A-0R6.

Abstract

Direct Numerical Simulations (DNS) are conducted to gain insight into the early ignition process in a non-homogeneous turbulent flow. This is the second part of a study to investigate the characteristics of renewable oxygenated fuel *versus* conventional diesel. In the first study, Unsteady Reynolds-Averaged Navier-Stokes (URANS) simulations of a research diesel engine were carried out. Attention was paid to the impact of the liquid phase properties on the in-cylinder flow patterns. DNS is employed here to investigate local micro-mixing effects on ignition. DiMethyl-Ether (DME) is the model for oxygenated fuel while conventional hydrocarbon (HC) is represented by n-heptane.

Subtle effects of micro-mixing are able to modify the combustion phasing in the compression-ignition mode. For the same temperature and mixture fraction distributions, the location of the stoichiometry iso-surface is different for the oxygenated and conventional fuels, and as a result ignition kernels develop at a higher temperatures for n-heptane than for DME. This may change the conclusions with respect to the cetane number and homogeneous ignition investigations.

Turbulence, ignition, DNS, complex chemistry, DME, diesel

Introduction

The main characteristics of biofuel esters are the presence of oxygen atoms set as an ester group, imparting polarity to one end of the molecule, and, often, one or more C=C double bonds (olefin groups). The number and the configuration of C=C double bonds (olefin groups) is a significant chemical feature. The major impact is a reduction of the heat release per unit mass. On the other hand, less oxidizer is required to burn a unit mass of an oxygenated

fuel. This compensates for the reduced heating value of the fuel. A flame temperature typical of hydrocarbons is preserved while more oxygen is available. This is recognized as favouring the formation of Zeld'ovitch NO_x. However, in practice, more fuel is injected to compensate for the loss in heat power. In the first part of this study, it was shown that biodiesel fuels tend to create a wider ignitable zone. This leads to large volumes of high temperature, likely to produce NO_x and carbon deposits. This is due to a longer distance of travel of droplets in the turbulent flow. On the other hand, ignition quality is also acknowledged as a key to emission control. A better understanding of the ignition process of oxygenated fuels compared to conventional hydrocarbons is thus of significant importance.

With improved computing resources, DNS of ignition in generic turbulent flows incorporating complex chemistry has become increasingly popular. Hydrogen (with ozone [1]) remains a fuel of preference, given the modest complexity of its chemistry [2-6]. Recently, a two-phase DNS of n-heptane ignition has been carried out [7,8]. DNS of n-heptane chemistry has also been achieved using a reduced mechanism in the framework of a mixing layer [9]. Direct simulation of turbulent combustion has been conducted with CO/H_2 chemistry [10] and reduced CH_4 chemistry [11]. The mechanism of pollutant formation in turbulent reacting flows has also been investigated with this approach [12]. In fields where details of chemistry are not mandatory, DNS has also been employed to address model development for turbulent flows [13-16] and flame sheet/turbulence interaction [17,18]. Other applications of DNS include fire studies [19-22], flame wall interaction [23], turbulence radiation interaction [24] and basic flame stabilization theories [25]. With the help of continuously increasing computer power, DNS is finding even broader ranges of application.

The objective of this study is to make use of DNS to gain insight into the processes of ignition in a non-homogeneous turbulent flow of an oxygenated fuel compared to a conventional hydrocarbon. The aim is to simulate

the early stages of diesel gas-phase ignition, in the limit of the resources inherent to DNS. Figure 1 illustrates the model schematically. Two representative fuels are employed for this purpose for which skeletal chemical mechanisms have been retained to diminish computer load. DiMethyl-Ether (DME) serves as a model for the oxygenated fuel (di-oxygenated alkyl), while n-heptane is used to represent conventional oil in the gas phase, as widely practised. The method, model problem and computational configuration are described in the following section. Results are discussed thereafter.

< Figure 1 >

Numerous DNS studies of turbulent combustion have provided a large amount of data. Some of these studies have been mentioned above. The present report is the second of a two-part study to investigate combustion of renewable oxygenated fuels. The first part was a CFD investigation of the in-cylinder combustion of conventional fuel and biodiesel. This second part attempts to overcome the limitations of URANS so as to obtain an improved understanding of micro-mixing and its effects on ignition, and hence on engine performance. It deals exclusively with normal-alkane and biodiesel fuels.

Model Problem

The chosen computational configuration is a 257^2-meshed 2-D square box for computational ease. The complex turbulent energy cascade is however a 3-D process in reality. This approximation should not lead to significant errors. The main difference between 2-D and 3-D turbulence energy cascade is the flux inversion. In a 2-D turbulent flow, small eddies tend to merge into larger structures such that the flow becomes self-organized

(something we have observed in our DNS). The main impact should be an under-estimation of micro-mixing in the general case. However, these DNS already address the tail of the turbulent spectrum. Even in 3-D, the smallest structures would have quickly disappeared. The longer survival of a weakly dissipative large structure in 2-D may tear apart the scalar pockets. This large advection motion is not supposed to have integral effects on chemistry. The initial non-homogeneous fields are carefully defined. Notice that 'non-homogeneous' is employed for the scalar distribution. It is not related to the nature of turbulence which is homogeneous and isotropic, energy-decreasing with time.

The turbulence (velocity and pressure) is imposed in terms of the integral length L and the root-mean-square velocity u'. The scalar field is imposed through the mean fuel mass fraction mixed with air and a segregation factor. The segregation factor is defined by $\sigma = Y_F'^2 / Y_F / (1-Y_F)$, in usual notations. A crude mixing law in temperature is built based on the relative concentrations of fuel Y_F and air Y_O and their respective temperatures T_F, and T_O.

$$T(\vec{r}) = T_F Y_F(\vec{r}) + T_O Y_O(\vec{r}) \tag{1}$$

where $\vec{r}$ is a position vector. This law of mixing approximates to the first order of the temperature fluctuations due to fuel vaporization in air. Such temperature fluctuations are also the expected local heterogeneities in a Homogeneous Charge Compression Ignition (HCCI) combustion chamber far from boundaries [26,27]. The mixture is represented by the multi-species ideal gas law.

The turbulent energy spectrum model is the Passot-Pouquet formalism [28], for a 2-D homogeneous turbulent field:

$$E(k) = \frac{32}{3}\sqrt{\frac{2}{\pi}}\frac{1}{k_o}\left(\frac{k}{k_o}\right)^4 e^{-2\left(\frac{k}{k_o}\right)^2} \tag{2}$$

k_o is the wave number at the maximum of the spectrum:

$$k_o = \frac{8}{3}\sqrt{\frac{2}{\pi}} \tag{3}$$

Distances are non-dimensionalized by the initial turbulence integral length scale L, and velocities by the initial turbulent mean square-root velocity u'. Other reference quantities are initial mean turbulent kinetic energy and Eddy-Turn-Over Time (ETOT, the characteristic time for an initial eddy to rotate, = L/u'). Temperature is kept in a dimensionalized form for ease.

A new DNS code, derived from an existing one [25], is employed to compute two-dimensional compressible conservation equations. This code has been designed to address complex transport and chemistry and to be adapted to non-shared memory machines and carrying radiation. Where possible, intensive re-employment of the source of the DNS code presented in [25] has been considered. The variables are density, velocity, total energy, and mass fractions of the species involved. The governing equations can be found in [29]. Complex mixture transport (including Soret effect) properties and relatively detailed chemistry are used. The species transport properties and chemistry are obtained using the TRANSPORT [30] and CHEMKIN-II packages [31], coupled to the DNS code. The numerical method is based on a sixth-order accurate implicit spatial differencing scheme [32]. Time integration is based on a third-order explicit Runge-Kutta time integration with low storage [33]. Boundary conditions are periodic.

The initial dynamic fields are the same in all the simulations. The turbulent Reynolds number ($Re_t = u'L\rho_o/\mu_o$, where ρ_o and μ_o are the initial mean density and dynamical viscosity in the domain) is about 22. The turbulent length scale is 0.08 of the box size. Consistently, the length scales of any initial scalar distribution are fixed as well.

They mimic a two-peak distribution whose wavelengths are 1.5 and 2.5. The first peak is chosen as a small wavelength scale compared to the turbulent energy spectrum peak (~2). It corresponds to coherent eddies breaking the pockets of scalar. The second one is in the inertial range and initiates micro-mixing. To match the statistic, a β-PDF function based on mean and segregation factor rescales the scalar field. The reader is referred to [34,35] for details of the initial condition definition used here. Typical pure fumigated fuel temperature is chosen as 500 K. Pure air temperature is adapted for different distributions such that the initial box average temperature is kept at 1100 K. This level of temperature has been chosen to be outside the range of the negative temperature coefficient range for ignition. A picture of the initial fields is provided in Fig. 2.

< Figure 2 >

The chemical schemes are the skeletal ones developed for n-heptane and DME ignition under engine-like conditions [36,37] at Chalmers University. These schemes are of the same family as the NASA Glenn Reduced Reaction Mechanisms for Generic Hydrocarbon Combustion [38-40]. In this type of scheme, the assumption is made of a single intermediate hydrocarbon fragment from which light HC chemistry is derived. The excessive computing demand leads to the use of these skeletal schemes, instead of more detailed ones. This is another limitation of the present simulations. N-heptane has a stoichiometry of 0.062, typical of saturated hydrocarbon fuels. On the other hand, DME has a much higher stoichiometry of 0.1 due to the oxygen atom. This is where, we believe, micro-mixing can have an impact and modify conclusions from homogeneous ignition investigations where only chemical kinetics are revealed.

0-D constant-volume ignition simulations (both with Senkin [31] and the present DNS code, for validation) of the proposed chemical schemes have exhibited under-prediction of the ignition delay The relative difference in ignition of DME with respect to n-heptane at 41 bars and 1100 K is nevertheless preserved. These schemes have eventually been adopted for DNS investigation due to the difficulty in finding reliable mechanisms for the types of fuel considered, and given the limited computer power available.

A highly dissipative mixture diminishes the numerical stiffness of chemistry. This leads to smooth ignition. This prevents combustion and acoustic coupling. These phenomena are beyond the scope of this study. The configuration mimics development of ignition kernels close to a diesel spray as sketched in Fig. 1. In that region, composition is not lean and dissipation is high based on experimental evidence. A globally low-Damkhöler chemistry in a highly-dissipative flow helps our computations while being still compatible with the study. Altered comprehensive mechanisms [17], or very lean mixtures [4] are other equivalent solutions practiced to emphasize some phenomena and diminishes the unwanted impact of others.

Five cases have been computed and they are reported in Table 1. Two cases have been simulated with DME and two with n-heptane. These four cases are at stoichiometry on average. Choice of cases close to stoichiometry is justified by observation in DI diesel engines. Experiments demonstrate that ignition occurs in regions where the mixture is close to stoichiometric. For each fuel, two segregation factors, $\sigma = 0.1$ and 0.2, are assumed. An additional case has been considered for an initial n-heptane rich mixture with $\phi = 1.68$ and $\sigma = 0.1$.

< Table 1 >

Computations have been carried out on two mesh size levels (129^2 and 257^2) and the results on the finest mesh are presented here. Minor differences (< 5%) were observed in the results, suggesting a sufficient resolution.

Results and Discussion

Contours of temperature and ignition-kernel-tracer species are shown for both DME (Case III) and n-heptane (Case I) in Fig. 3 after five ETOT. According to these pictures (and within the limit of the chemical description permitted by the mechanism used), OH radicals correlate reasonably well with the hottest spots, pointing out the mixture in ignition. As shown in the figure, this tracer is more visible in the case of DME than n-heptane, because of a slower and more localized ignition for n-heptane. When the same advancement in ignition is considered (*i.e.,* the same mean temperature and no more time advancement to pick up a field), OH radical pockets clearly appear within the ignition kernels as well for n-heptane (not shown here), with the same order of magnitude.

<Figure 3>

The intermediate species field is another marker to monitor the course of ignition. According to [36,37], the representative intermediate species is CH_2O in the DME chemical scheme while a direct decomposition into CO can be approximated for n-heptane. On the basis of these proposed schemes, the area of initiation of oxidation of both fuels is provided in Fig. 4 at the same time for Case III and I as above. The intermediate species are thus good markers of the advancement of the ignition phase [7]. At first, they are the signature of the decomposition of the molecule. When ignition is more advanced, they are consumed. These are the reasons why the intermediate species maps do not correlate perfectly with the temperature maps, Fig.3, but together they provide a comprehensive pattern of chemical state. Once again, DME experiences a rapid ignition and the ignition kernels develop well in regions of high scalar dissipation, as observed in the lower part of the domain, Fig 5.

<Figure 4>

<Figure 5>

The effects of micro-mixing on ignition are illustrated in Fig. 6. It exhibits the averaged temperature runaway in the course of ignition for the five simulated cases. First, the advantage of having chosen a high dissipation field is highlighted: the time-evolution of the temperature is slow enough to detect all the embedded phenomena. The most important one is the effect of micro-mixing temperature, i.e. the temperature evolution at the scale of the computational domain where all the turbulent structures are solved. When the segregation is large enough, ignition is very slow such that the effect of mixing temperature is visible. The mixing temperature is the final temperature after the homogenization of a mixture initially segregated in composition and temperature. The final mixing temperature in the flow without combustion would be lower than the initial mean temperature. This is due to the homogenisation of a mixture composed of cold fuel and hot air with different heat capacities. This cooling delays ignition, as evidenced by the initial decreasing trend of the temperature for the highest value of σ. This phenomenon is not visible for the lower segregation because: (i) temperature runaway hides it; and (ii) ignition is fast enough to prevent this cooling process such that the combustion chemistry is never affected by it. Note that conditions here are outside the range of the negative temperature coefficient ignition and there is no benefit of a lower temperature due to mixing. Note also that different reactants will lead to different heat capacities and hence different results.

<Figure 6>

Another interesting aspect is the comparison between the DME and n-heptane ignitions for the same initial field (i.e. the mixture is stoichiometric for DME but rich for n-heptane). These are Cases III (stoichiometric DME) and V (rich n-heptane). N-heptane ignition benefits for two reasons: (i) n-heptane ignites easier in rich mixtures; (ii) in this typical inhomogeneous field, n-heptane concentration iso-lines are pushed towards hot pockets of air. This is due to the difference in the stoichiometry between DME (0.1) and n-heptane (0.062).

Figure 7 gives a comparative sequence with time of the ignition of the stoichiometric mixture (Case I) *versus* the rich mixture for n-heptane (Case V) for the first ten ETOT. It is seen that hot temperature spots are initially on the lean side and very close to stoichiometry, due to the higher air temperature. However, these spots quickly switch to the rich side with time. On these figures, the white iso-line delineates the position of stoichiometry composition. Stoichiometry is established thanks to the mixture fraction based on the carbon mass fraction, as complex transport precludes the use of conventional mixture fraction. The number with white background indicates the hot spot local temperature. The number with no background points to the very cold and rich pocket of fuels which fail to ignite. It must be noticed that, although the rich mixture (Case V) ignites faster, the ignition is achieved in a more segregated way. The cold rich kernel (due to a high local concentration of the cold fuel pockets) fails to ignite in the rich case while all the rich cold spots eventually disappear in the stoichiometric case.

< Figure 7 >

Thus, when the mixture is rich, inhomogeneities support ignition of conventional hydrocarbon fuels. This behaviour is well illustrated in Fig.8 which displays the heat release rate of the generic initial field for Case I and Case V. The white line is the stoichiometry contour and the black line is for an equivalence ratio of about 10. Two observations

are made from these pictures. (i) The area at high heat release is larger for the rich case, due to larger pocket of fuels. The rich ignitable mixture is thus more widespread. (ii) For Case V, iso-equivalence-ratios are in the higher temperature zone compared to Case I. This leads to an ignition zone shifted towards the rich side (farther from the white line but closer to the black line). This situation is suspected to happen with the increase of load in diesel engines and is a potential explanation for the observed decreasing discrepancies in ignition time between biodiesel esters and conventional diesel when more fuel is injected [41]. For fatty esters, a higher cetane number advances the combustion phasing in an 0-D type configuration like a combustion bomb. However, in engines this advancement disappears at high load, and esters and hydrocarbons both tend to ignite at similar times, according to cylinder data.

< Figure 8>

Conclusion

It has been shown that turbulent mixing in a non-homogeneous field may impact ignition processes of oxygenated fuels. DME, has a relatively large cetane number compared to normal alkane oils. However, the shift in the stoichiometric value makes it ignite and burn in colder regions while classical hydrocarbons tend to react on the hot air side. This pattern may explain, at least in part, why the benefit in ignition of biodiesel esters disappears with the load in a diesel engine, compared to n-alkane.

The scalar dissipation rate has the expected qualitative effect. A higher segregation factor delays ignition. This is primarily due to heat loss from the combustion zone. Moreover, another effect concerns the accelerated mixing. Because of the difference in heat capacity, there exists a mixing temperature for a cold fuel but hot air mixture. If this temperature is lower than the averaged one, it may impact ignition. The mean temperature in the box may not

be representative for the ignition process if this latter is slow compared to micro-mixing. This effect is different and additive to the dissipation heat loss. Both are enhanced by a higher dissipation. This subtle effect may have to be considered in improved combustion models dedicated to HCCI engines as well. Combustion phase is very hard to control.

This study may also be beneficial for HCCI combustion (evidences of micro-mixing effects around non-homogeneous spots in competition with pure kinetics poses challenges for modelling) although the present configuration is not really close to a typical HCCI one. Methanol is a good candidate for HCCI engines as a renewable fuel. Its tolerance to Exhaust Gas Recirculation (EGR) is an interesting feature. Its high octane number might be controlled through the use of reformate gas. Further work is planned to investigate self-ignition in turbulent non-homogeneous fields of methanol-reformate gas in hot air at high pressure.

Acknowledgement

This research has been made possible by the funding received from the Government of Canada Program for Energy Research and Development (PERD/AFTER) and from the National Research Council of Canada.

The contribution from Dr W. Wallace to improve the shape of the communication is greatly appreciated.

Contact

Joan-André Boulanger, National Research Council of Canada, Institute for Aerospace Research, Building M-10 Room 104, 1200 Montréal Road, K1A 0R6 Ottawa, Ontario, Canada. Ph.: 1 613 949 7687. Fx: 1 613 952 7677. E-mail: Joan.Boulanger@nrc-cnrc.gc.ca

References

[1] de Charentenay, J., Thévenin, D. and Zamuner B., 2002, Comparison of direct numerical simulations of turbulent flames using compressible or low-Mach number formulations, *International Journal of Numerical Method in Fluids* **39** 497-515.

[2] Chen, J., Hawkes, E., Sankaran, R., Mason, S. and Im, H., 2006, Direct numerical simulation of ignition front propagation in a constant volume with temperature inhomogeneities. i fundamental analysis and diagnostic, *Combustion and Flame* **145** 128-44.

[3] Hawkes, E., Sankaran, R., Pébay, P. and Chen, J., 2006, Direct numerical simulation of ignition front propagation in a constant volume with temperature inhomogeneities. ii. parametric study, *Combustion and Flame* **145** 145-59.

[4] Sankaran, R., Im, H., Hawkes, E. and Chen, J., 2004, The effects of non-uniform temperature distribution on the ignition of a lean homogeneous hydrogen-air mixture, in: *Proc. Combustion Institute*.

[5] Echekki, T. and Chen, J., 2003, Direct numerical simulation of autoignition in non-homogeneous hydrogen-air mixtures, *Combustion and Flame* **134** 169-91.

[6] Baum, M., Poinsot, T.J., Haworth, D.C. and Darabiha, N., 1994, Direct numerical simulation of $H_2/O_2/N_2$ flames with complex chemistry in two-dimensional turbulent flows, *Journal of Fluid Mechanics* **281** 1-32.

[7] Wang, Y. and Rutland, C., 2004, Effects of temperature and equivalence ratio on the ignition of n-heptane fuel spray in turbulent flow, in: *Proc. Combustion Institute*.

[8] Wang, Y. and Rutland, C., 2005, DNS study of the ignition of n-heptane fuel spray under high pressure and lean conditions, in: *J.o.P.: Conference Series*, Institute of Physics Publishing.

[9] Viggiano, A. and Magi, V., 2004, A 2-D investigation of n-heptane autoignition by means of direct numerical simulation, *Combustion and Flame* **137** 432-43.

[10] Hawkes, E.R., Sankaran, R., Sutherland, J.C. and Chen, J.H., 2005, Direct numerical simulation of turbulent combustion: fundamental insights towards predictive models, in: *J.o.P.: Conference Series*, Institute of Physics Publishing.

[11] Hawkes, E.R. and Chen J.H., 2006, Comparison of direct numerical simulation of lean premixed methane-air flames with strained flame calculations, *Combustion and Flame* **144** 112-25.

[12] Bédat, B., Egolfopoulos, F. and Poinsot, T., 1999, Direct numerical simulation of heat release and NO_x formation in turbulent nonpremixed flames, *Combustion and Flame* **119** 69-83.

[13] Luo, K.H., 1999, Combustion effects on turbulence in a partially premixed supersonic diffusion flame, *Combustion and Flame* **119** 417-35.

[14] Le Ribault, C., Le Penven, L. and Buffat, M., LES of the compressed Taylor vortex flow using a finite volume/finite element method on unstructured grids, *International Journal for Numerical Methods in Fluids*, In Press.

[15] Rahman, M. M., Siikonen, T., 2005, An eddy viscosity model with near-wall modifications, *International Journal for Numerical Methods in Fluids* **49** 975-97.

[16] Sergent, A., Joubert, P., and Le Quéré, P., 2003, Development of a local subgrid diffusivity model for Large-Eddy Simulation of buoyancy-driven flows: application to a square differentially heated cavity, *Numerical Heat Transfer: Part A: Applications* **44** 789-810.

[17] Sreedhara, S. and Huh, K.Y., 2005, Assessment of closure schemes in second-order conditional moment closure against DNS with extinction in ignition, *Combustion and Flame* **143** 386-401.

[18] Jenkins, K.W., Klein, M., Chakraborty, N. and Cant, R.S., 2006, Effects of strain rate and curvature on the propagation of a spherical flame kernel in the thin-reaction-zones regime, *Combustion and Flame* **145** 415-34

[19] Jiang, X. and Luo, K.H., 2000, Combustion-induced buoyancy effects of an axisymmetric reactive plume, in: *Proc. Combustion Institute*.

[20] Jiang, X. and Luo, K.H., 2001, Spatial DNS of flow transition of a rectangular buoyant reacting free-jet, *Journal of Turbulence*, **2**, 1-15.

[21] Jiang, X. and Luo, K.H., 2000, Spatial direct numerical simulation of the large vortical structures in forced plumes, *Flow, Turbulence and Combustion* **64** 43-69.

[22] Boulanger, J., Liu, F. and Smallwood G.J., 2006, Buoyancy-driven structures on jet diffusion flames, in: *Proc. Combustion Institute Canadian Section Spring Technical Meeting*.

[23] Wang Y., 2005, Direct Numerical Simulation of Non-premixed Combustion with Soot and Thermal Radiation, Ph.-D. dissertation.

[24] Wu, Y., Haworth, D.C., Modest, M.F. and Cuenot B., 2005, Direct numerical simulation of turbulence/radiation interaction in premixed combustion systems, in: *Proc. Combustion Institute*.

[25] Boulanger, J., Vervisch, L., Réveillon, J. and Ghosal S., 2003, Effects of heat release in laminar diffusion flames lifted on round jets, *Combustion and Flame* **134** 355-68.

[26] Kong, S.C., and Reitz, R.D., 2002, Application of delailed chemistry and CFD for predicting direct injection HCCI engine combustion and emissions, in: *Proc. Combustion Institute*.

[27] Kong, S.C. and Reitz, R.D., 2003, Numerical study of premixed HCCI engine combustion and its sensitivity to computational mesh and model uncertainities, *Combustion Theory and Modelling* **7** 417-33.

[28] Hinze, J. O., 1975, Turbulence, McGraw-Hill, New York.

[29] Kuo, K., 1986, Principles of combustion, John Wiley and sons, New York,.

[30] Kee, R.J., Dixon-Lewis, G., Warnatz J., Coltrin M.E. and Miller, J.A., 1986, A Fortran computer code package for the evaluation of gas-phase, multicomponent transport properties, *Technical Report*, SAND86-8246, Sandia National Laboratories.

[31] Kee, R.J., Rupley, F.M. and Miller, J.A., 1989, Chemkin-II: A Fortran chemical kinetics package for the analysis of gas-phase chemical kinetics, *Technical report* SAND89-8009B, UC-706, Sandia National Laboratories.

[32] Lele, S., 1992, Compact finite difference schemes with spectral like resolution, *Journal of Computational Physics* **103** 16-42.

[33] Wray, A., 1990, Minimal storage time - advancement schemes of spectral methods, *Technical report*, Center for Turbulence Research, Stanford University, Stanford, CA-USA.

[34] Réveillon, J., 1996, Simulation dynamique des grandes structures appliquée aux flammes turbulentes non-prémélangées, Ph.-D. thesis, Université de Rouen, Rouen, France - EU.

[35] Vervisch-Guichard, L., 1999, Développement d'outils numériques dédiés à l'étude de la combustion turbulente, Ph.D. thesis, Université de Rouen, Rouen, France - EU.

[36] Nordin, N., and Golovitchev, V., 1997, Numerical evaluation of n-heptane spray combustion at diesel-like conditions, in *Proc. The 7th International KIVA Users Meetings, SAE Congress*.

[37] Golovitchev, V., Nordin, N., and Chomiak, J., 1997, Numerical evaluation of dual oxygenated fuel setup for DI diesel application, in *Proc. SAE International Spring Fuels & Lubricants Meeting & Exposition*.

[38] Kundu K.P., Penko P.F. and Yang S.L., 1998, Simplified Jet-A/Air combustion mechanisms for calculation of NO_x emissions, in *Proc. 34th AIAA/SME/SAE/ASEE Joint Propulsion Conference and Exhibit*.

[39] Kundu K.P., Penko P.F. and VanOverbeke T.J., 1999, A practical mechanism for computing combustion in gas turbine engines, in *Proc. 35th AIAA/ASME/SAE/ASEE Joint Propulsion Conference and Exhibit*.

[40] Lee, C.-M., Kundu K. and Acosta W., 1991, Jet-A reaction mechanism study for combustion application, in *Proc. 27th AIAA/SAE/ASME/ASEE Joint Propulsion Conference and Exhibit.*

[41] Sinha, S., and Agarwal, A. K., 2006, Combustion characteristics of rice bran oil derived biodiesel in a transportation diesel engine, in *Proc. ASME-ICES 2006*.

List of Figures

Note that Black & White figures are available for editorial concerns.

white background: temperature (in K) hot spots. Number with transparent background: fuel mass fraction in cold pockets.

Fig. 8. Heat Release rate at initial time. (a) Case I. (b) Case V. White line: stoichiometry. Black line: equivalence ratio equal to ten.

Tab. 1. Table presenting the different test cases.

	Φ	σ	DME	N-heptane
I	1.	.1		x
II	1.	.2		x
III	1.	.1	x	
IV	1.	.2	x	
V	1.68	.1		x

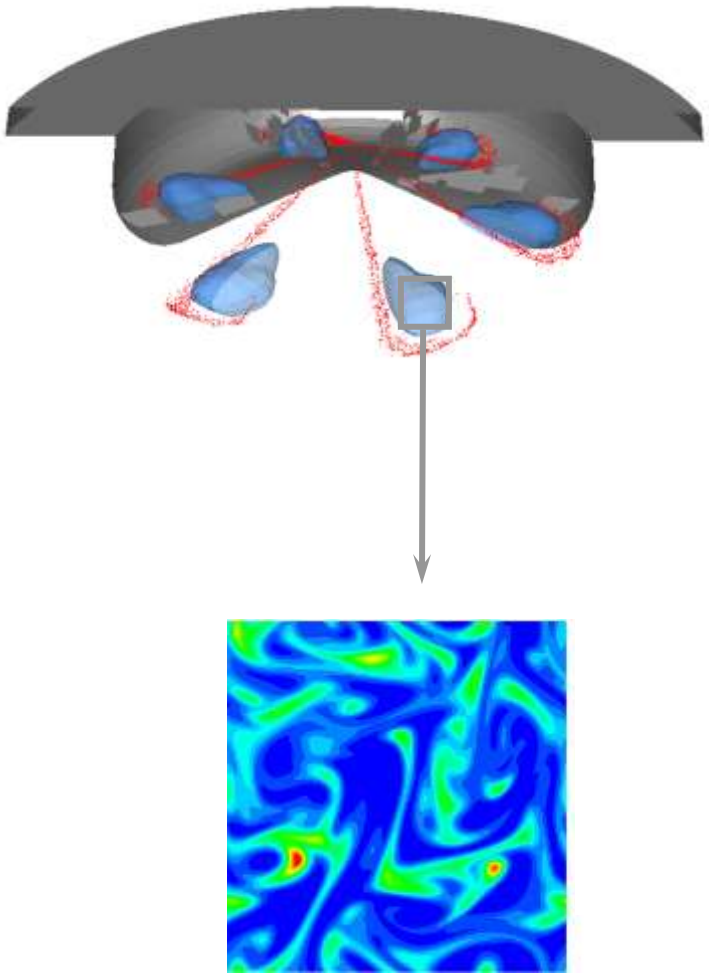

Fig. 1. Sketch of the ignition zone on the side of the spray

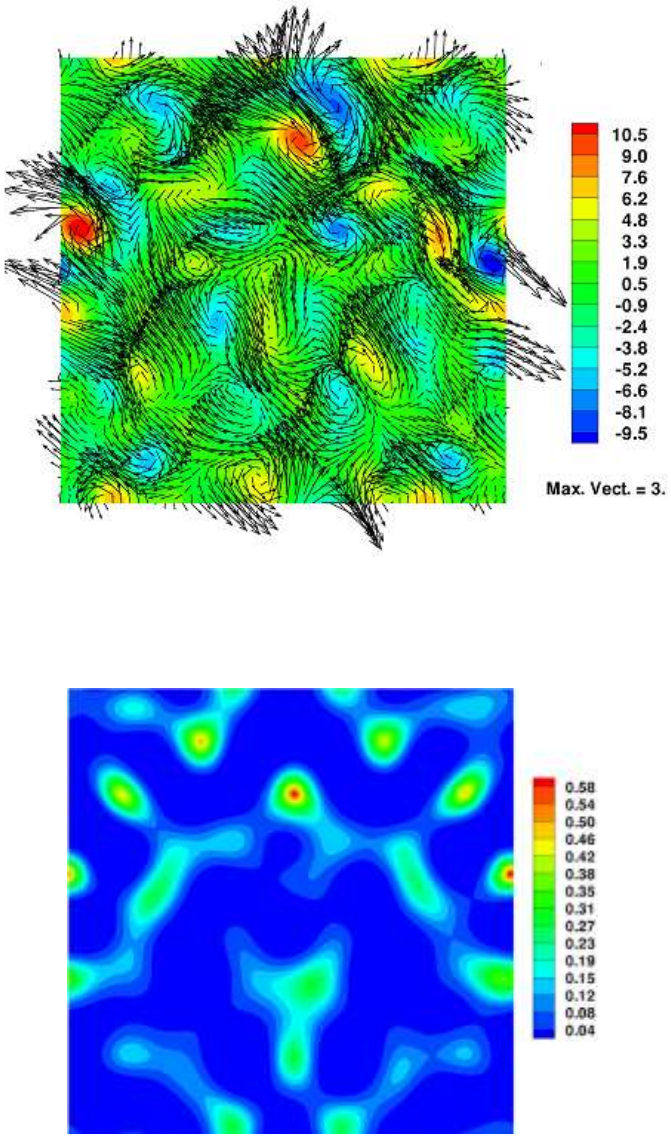

Fig. 2. Initial fields. Top: vorticity (arrows: velocity). Bottom: mixture fraction. Case I.

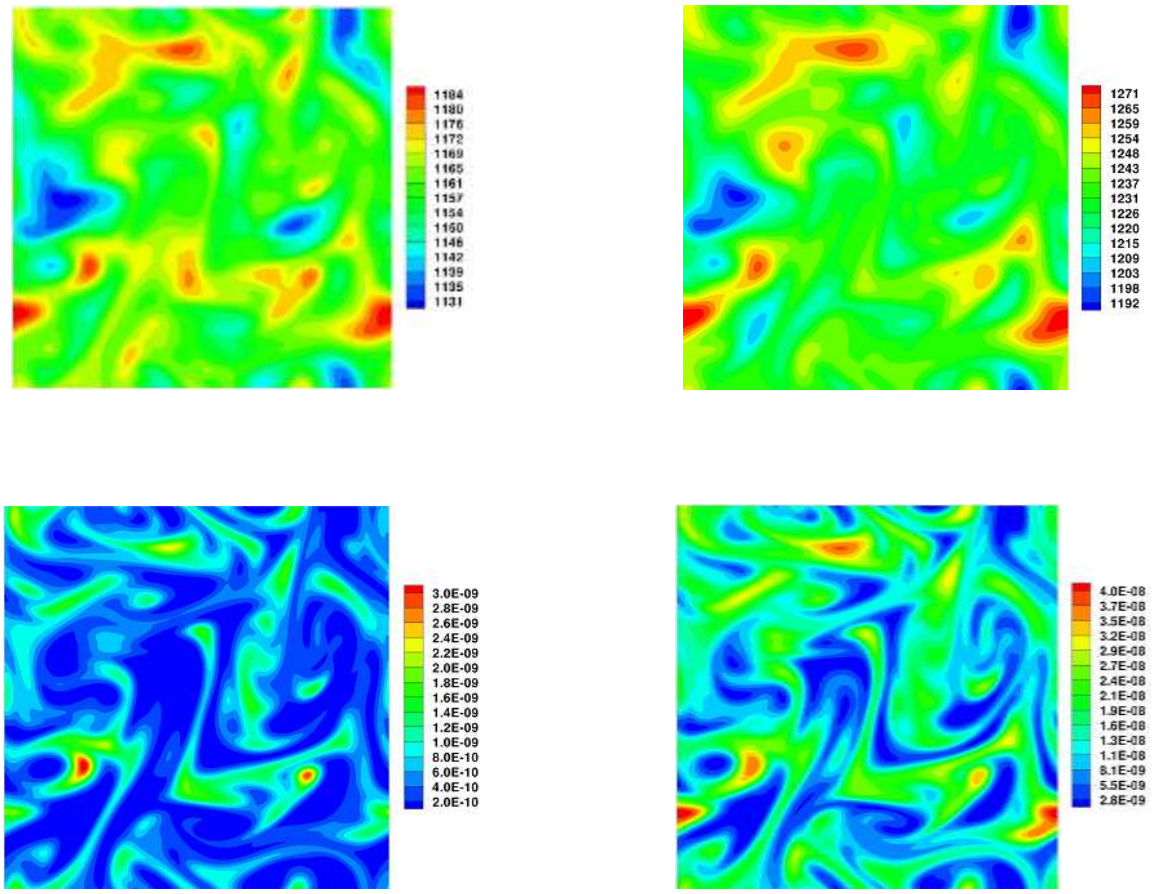

Fig. 3. Temperature (top) and OH radical (bottom) fields for n-heptane – Case I (left) and DME – Case III (right) after five ETOT.

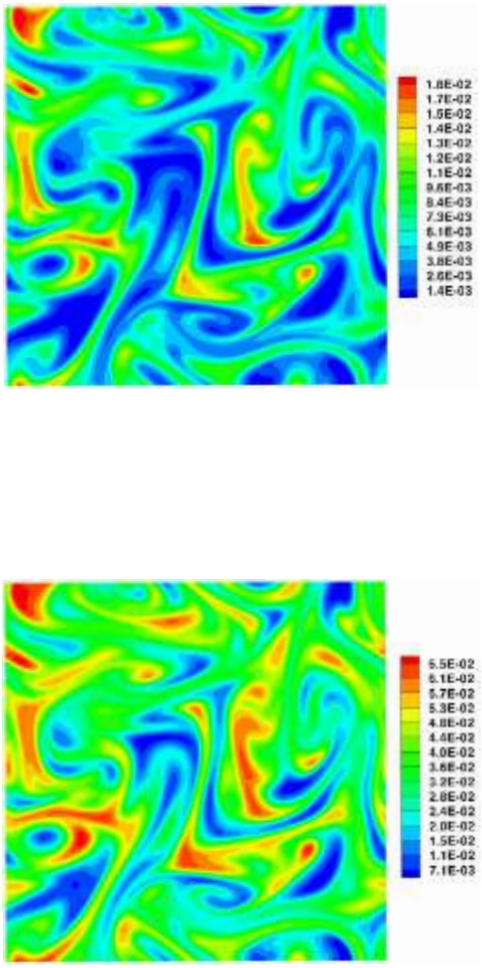

Fig. 4. Mass fraction of CO / n-heptane – Case I (top) and CH_2O / DME – Case III (bottom) after five ETOT

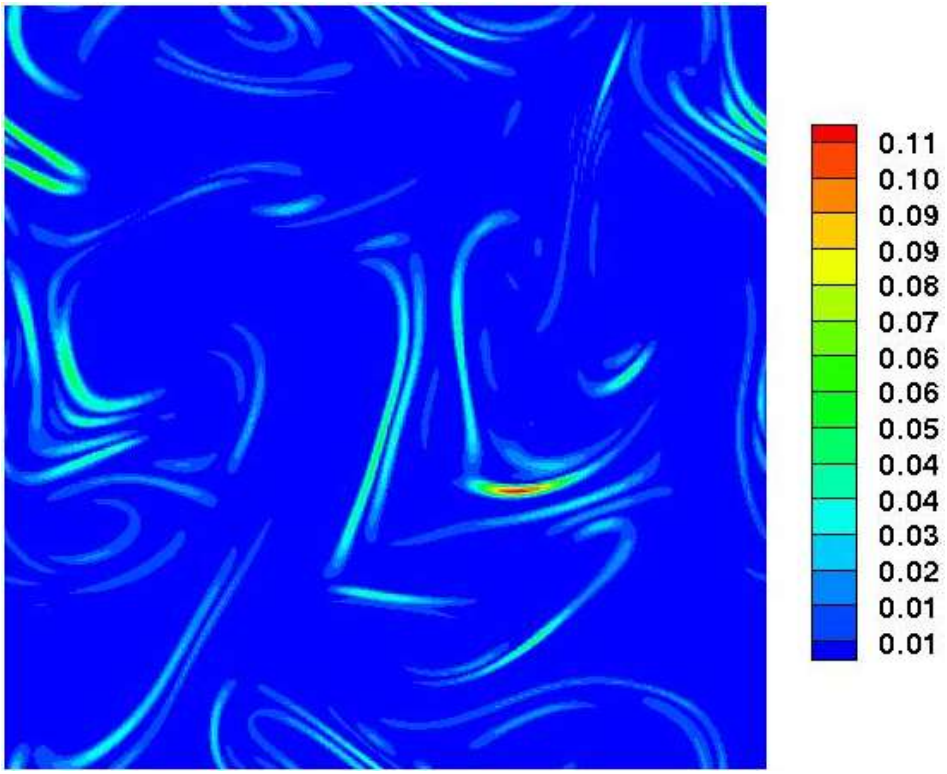

Fig. 5. Scalar dissipation rate for Case I after five ETOT.

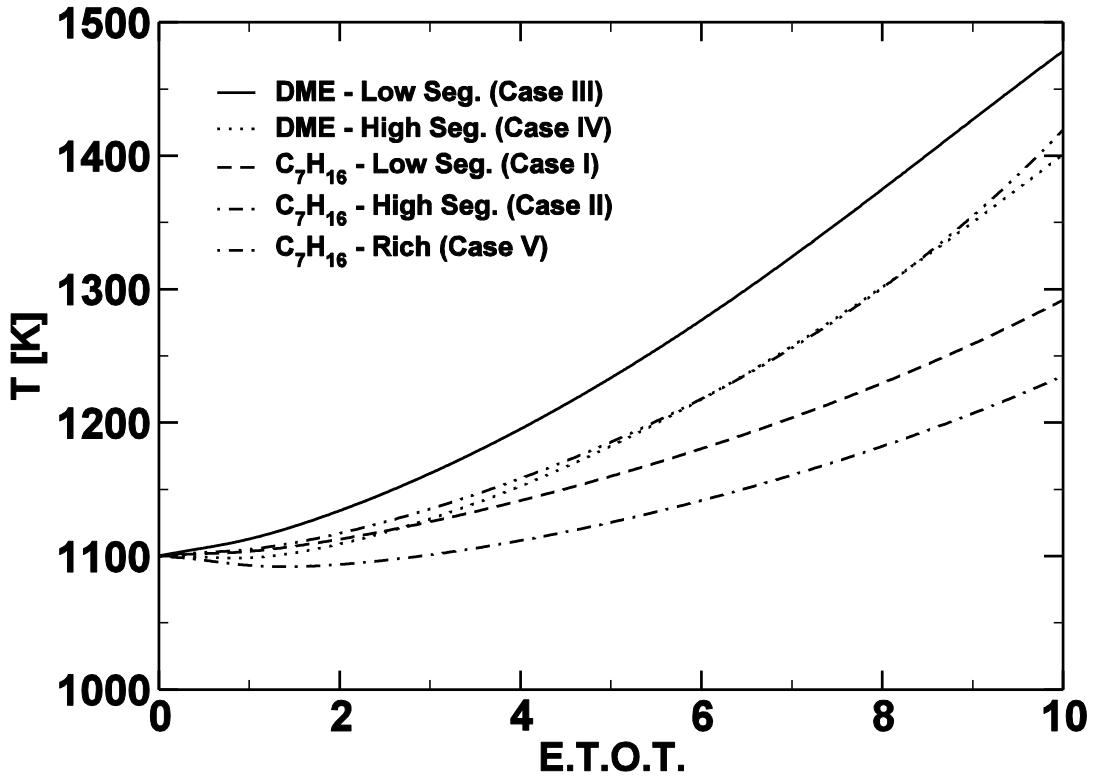

Fig. 6. Mean temperature *versus* time for different initial fields and fuels corresponding to Tab. 1

(a)

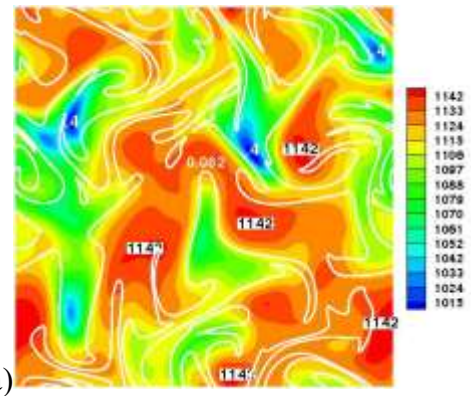
1142
1133
1124
1115
1106
1097
1088
1079
1070
1061
1052
1042
1033
1024
1015
1142
1142
1142
1142
1142
1142

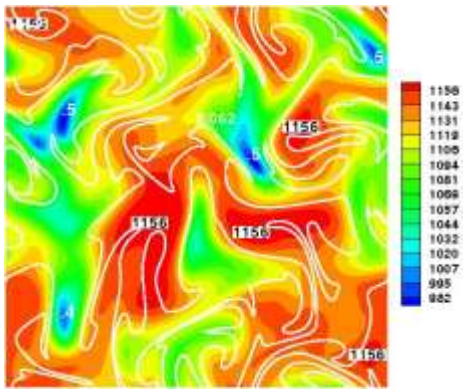
1156
1143
1131
1118
1105
1094
1081
1069
1057
1044
1032
1020
1007
995
982
1156
1156
1156
1156

(b)

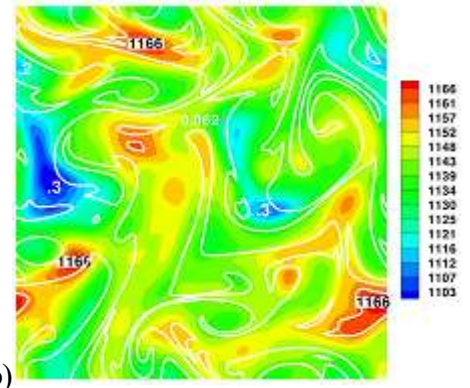
1166
1161
1157
1152
1148
1143
1139
1134
1130
1125
1121
1116
1112
1107
1103
1166
1166
1166
1166

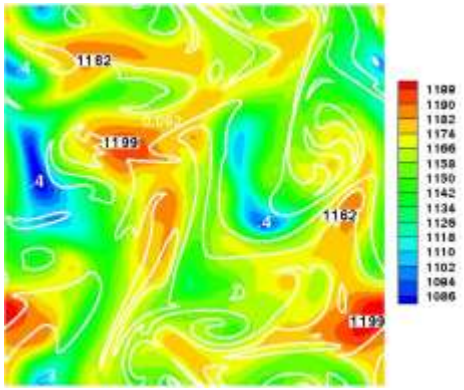
1189
1190
1182
1174
1166
1158
1150
1142
1134
1126
1118
1110
1102
1094
1086
1182
1199
1182
1199

(c)

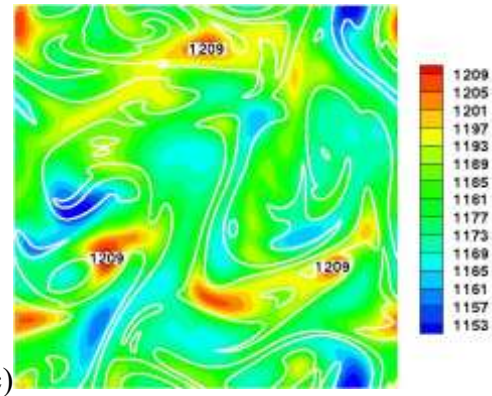
1209
1205
1201
1197
1193
1189
1185
1181
1177
1173
1169
1165
1161
1157
1153
1209
1209
1209

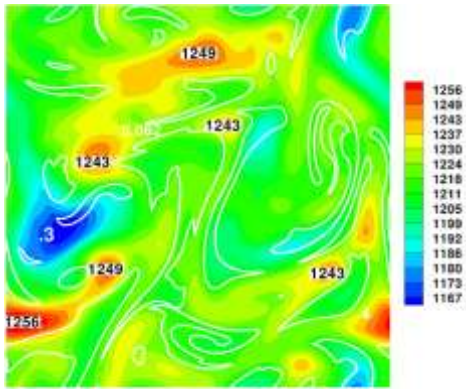
1256
1249
1243
1237
1230
1224
1218
1211
1205
1199
1192
1186
1180
1173
1167
1249
1243
1243
1249
1243
1256

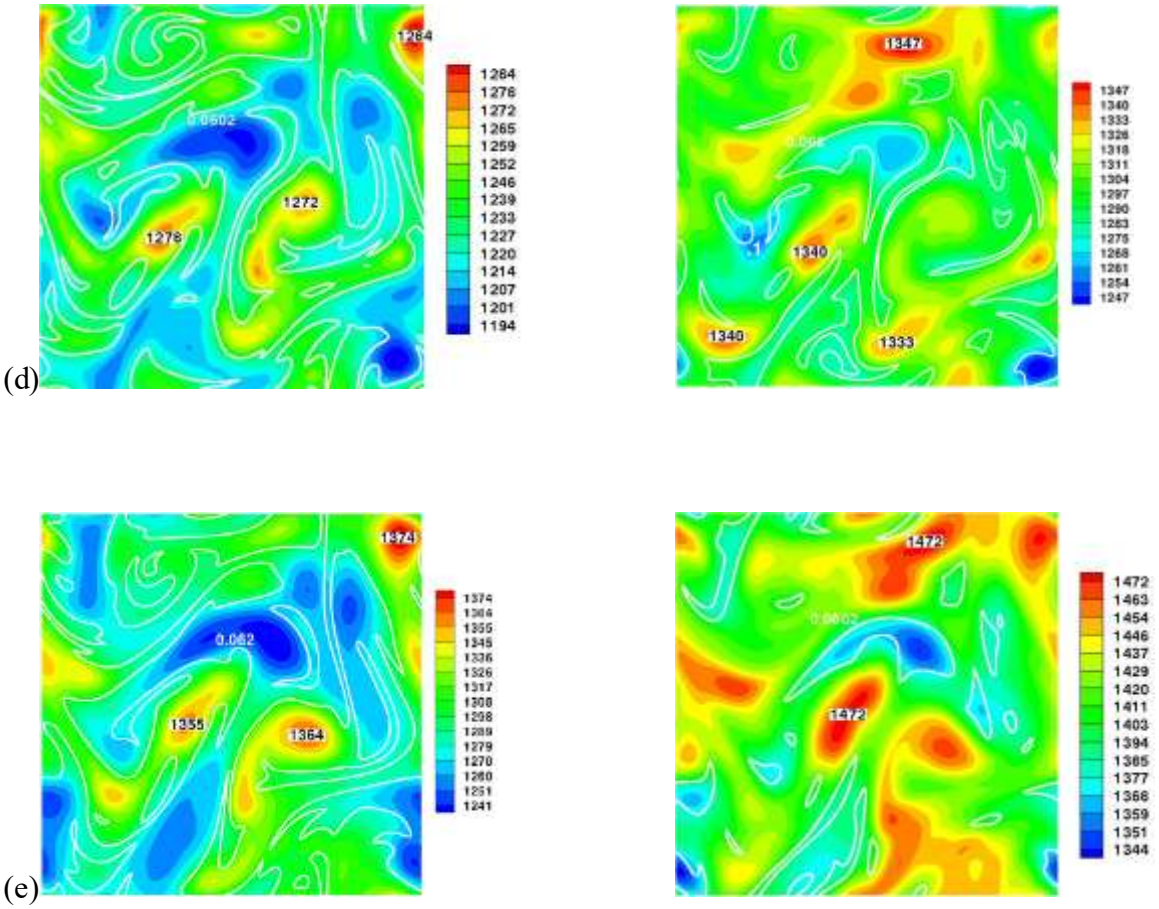

Fig. 7. Comparative simulations of DNS ignition for cases I (right) and case V (left). (a) after 2 ETOT. (b) after 4 ETOT. (c) after 6 ETOT. (d) after 8 ETOT. (e) after 10 ETOT. White line: stoichiometry (0.062). Number with white background: temperature (in K) hot spots. Number with transparent background: fuel mass fraction in cold pockets.

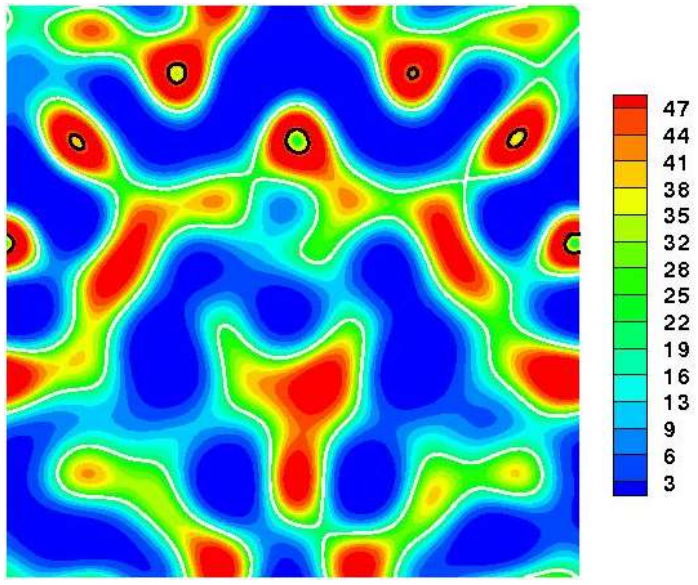

(a)

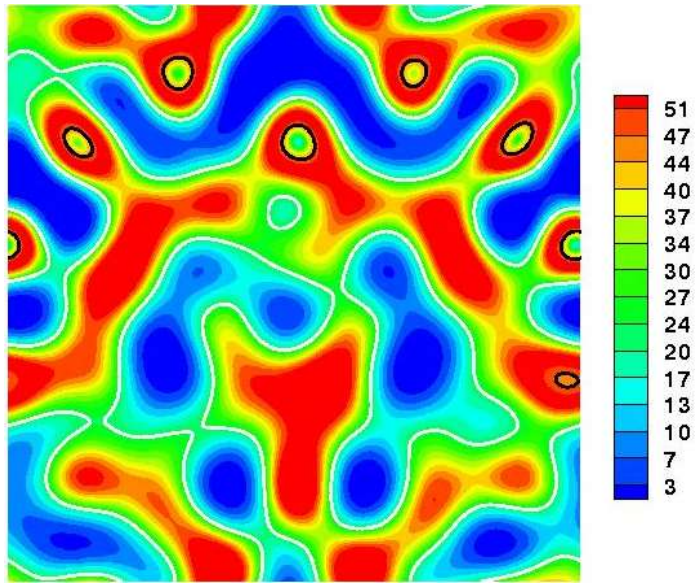

(b)

Fig. 8. Heat Release rate at initial time. (a) Case I. (b) Case V. White line: stoichiometry. Black line: equivalence ratio equal to ten.